Signature of linear-in-*k* Dresselhaus splitting in the spin relaxation of *X*-valley electrons in indirect band gap AlGaAs

Priyabrata Mudi,[1,2,*] Shailesh K. Khamari,[1] Joydipto Bhattacharya,[2,3] Aparna Chakrabarti,[2,3] and Tarun K. Sharma[1,2,†]

[1]*Semiconductor Materials Lab, Materials Science Section, Raja Ramanna Centre for Advanced Technology, Indore 452013, Madhya Pradesh, India*

[2]*Homi Bhabha National Institute, Training School Complex, Anushakti Nagar, Mumbai 400094, Maharashtra, India*

[3]*Theory and Simulations Laboratory, HRDS, Raja Ramanna Centre for Advanced Technology, Indore 452013, Madhya Pradesh, India*

(Received 20 July 2021; revised 8 August 2021; accepted 26 August 2021; published 9 September 2021)

The GaAs/AlGaAs quantum well (QW) system is utilized to investigate the electron spin relaxation in the satellite *X* valley of indirect band gap $Al_{0.63}Ga_{0.37}As$ epitaxial layers through polarization-resolved photoluminescence (PL) excitation spectroscopy. Solving the rate equations, steady-state electronic distribution in various valleys of $Al_xGa_{1-x}As$ is estimated against continuous photocarrier generation, and an expression for the degree of circular polarization (DCP) of PL coming from the adjacent QW is derived. Amalgamating the experimental results with analytical expressions, the *X*-valley electron spin relaxation time (τ_S^X) is determined to be 2.7 ± 0.1 ps at 10 K. To crosscheck its validity, theoretical calculations are performed based on density functional theory within the framework of the projector augmented wave method which support the experimental result quite well. Further, temperature dependence of τ_S^X is studied over 10–80 K range, which is explained by considering the intravalley scattering of carriers and Dyakonov-Perel spin relaxation in the *X* valley of the indirect band gap AlGaAs barrier layer. It is learned that the strain-induced modification of band structure lifts the degeneracy in the *X* valley, which dominates the electron spin relaxation <50 K. Furthermore, the DCP spectra of hot electrons in indirect band gap AlGaAs layers are found to be significantly different than that of direct bandgap AlGaAs. It is understood as a signature of linear *k*-dependent Dresselhaus spin splitting and the faster energy relaxation procedure in the *X* valley.

DOI: 10.1103/PhysRevB.104.115202

I. INTRODUCTION

For a significant amount of time, the spin dynamics of photogenerated electrons in III–V semiconductors has gained substantial curiosity of researchers due to its applications in the development of fast and high-performance spin-optoelectronic devices [1–5]. Following the work of Dyakonov and Perel [6], researchers have developed an understanding of the electron spin dynamics in III–V semiconductors both theoretically as well as experimentally [6–12]. The theoretical substructure of spin optoelectronics was developed based on density functional theory (DFT) and 14- to 34-band **k**·**p** theory [6,9,10]. On the other hand, the experimental development of electron spin dynamics was extensively established through polarization and time-resolved photoluminescence (PL) spectroscopy, inverse spin Hall effect, and Kerr rotation microscopy [13–15]. Interestingly, most of these works are restricted to the near band-edge region of direct band gap III–V semiconductors. However, for practical implications of spintronic devices, like spin light emitting devices and spin lasers, satellite valleys play a pivotal role since these devices operate under high-bias conditions where electrons in general occupy all three valleys (Γ, *L*, and *X*) [16,17]. Further, an immense spin-orbit coupling is also predicted in the satellite valleys as *p*- and *d*-type orbitals from the higher bands overlap with the conduction band orbital wave function at higher *k* values and are expected to influence its nature [18]. Based on this, Okamoto *et al.* [19] explored the *L*-valley electron spin dynamics in *n*-GaAs through inverse spin Hall effect by predicting a huge spin Hall angle. Furthermore, linear *k*-dependent spin splitting and high Lande *g* factor of electrons are the two important features of satellite valleys that could help in improving the performance of spintronic devices. Due to these reasons, spintronic devices fabricated based on the satellite valleys of III–V semiconductors have caught the attention of the research community in recent times [16,20–22]. Nonetheless, Joule heating in the device due to application of high bias is one of the major drawbacks in their practical implication [20]. Further, a steep fall of spin relaxation time is seen under high bias [19], as electrons are transferred to the satellite *L* valleys, where the reported value of spin relaxation time (τ_S^L) is very short [22]. Recently, it was discovered that one can optically inject spin-polarized electrons in the satellite *L*-valleys of GaAs and AlGaAs [22,23]. This could become a powerful tool in overcoming the Joule heating problem since the satellite valleys are now optically accessible. Amid the importance of optical spin injection in the satellite valleys, this technique is seldom discussed in the literature. The main reason behind this lies in the direct band gap nature of most of III–V semiconductors, where only a very small fraction of photogenerated carriers occupies the higher satellite valleys. In this regard, indirect bandgap semiconductors like $Al_xGa_{1-x}As$ ($x > 0.4$) provide an excellent opportunity since their satellite *X*-valley minima

*mudi@rrcat.gov.in, priyabratamudi63@gmail.com
†tarun@rrcat.gov.in

lie at lower energy than Γ-valley minima. Therefore, despite photo-injection in Γ valley, most of the electrons thermalize to satellite valleys within tens of femtoseconds [24], even in the absence of applied bias. Further, AlGaAs is almost lattice matched to GaAs, and high-quality epitaxial layers can be easily grown on GaAs wafers by growth techniques like metal organic vapor phase epitaxy (MOVPE) and molecular beam epitaxy. Nevertheless, fabrication of spin-photonic devices requires a complete knowledge of optical spin injection process, spin dynamics, and spin relaxation time in that material. Thus, a knowledge of the spin relaxation time of electrons in satellite valleys is extremely important to optimize the performance of associated devices. Zhang *et al.* [22] have determined the spin relaxation time of electrons in the *L*-valley of GaAs through time-and polarization-resolved PL excitation (PLE) spectroscopy. They have estimated this value to be as short as 0.2 pico-second, confirming the enhancement of the Dyakonov-Perel (D-P) spin relaxation mechanism due to large Dresselhaus spin splitting. Recently, spin relaxation in the *X* valley of AlAs was studied for those electrons which are bound to the holes situated in the GaAs quantum well (QW; type II band alignment) forming a spatially indirect exciton [25,26]. Further, *X*-valley spin relaxation of electrons was investigated in (In,Al)As/AlAs quantum dots (QDs; type I band alignment) at low temperatures [27–31]. In both cases, electrons are localized in space, and the wave vector k is not a good quantum number. As a result, mechanisms which dominate the spin relaxation for delocalized electrons, like D-P and Elliot-Yafet (E-Y) processes are suppressed. It is important to point out that no information is available on the spin relaxation of electrons in the *X* valley of the bulk AlGaAs barrier which are essentially delocalized. Thus, optical spin-orientation spectra as well as the spin relaxation time of electrons in the *X* valley (τ_S^X) of indirect AlGaAs needs to be evaluated before its spin-photonic applications. Notably, throughout this paper, the term spin relaxation of electrons refers to the delocalized electrons which are dominated by the D-P mechanism.

As pointed out earlier, in the case of direct bandgap semiconductors, optical orientation of electrons is investigated through polarization-resolved PLE spectroscopy by measuring the degree of circular polarization (DCP) of PL as a function of excitation energy. Though this technique is nondestructive in nature, it is irrelevant for indirect bandgap semiconductors due to the suppression of radiative processes that gives rise to a weak PL signal at low temperature. Even though the magnitude of indirect band gap PL increases with temperature, any possible advantage because of this is shadowed by a simultaneous reduction of spin relaxation time [13]. Thus, a high-intensity tunable laser source may be required to increase the PL magnitude, which will allow the measurement of a few percent of the DCP of the signal. However, use of high-intensity laser sources to increase the PL intensity will not be of much help as electron spin dynamics itself depends on the intensity of the excitation source [14]. In this context, GaAs/AlGaAs QWs offer a credible system to investigate the optical orientation properties of electrons in the barrier layer using low-intensity light sources. In our previous work [23], we have employed GaAs/AlGaAs multi-QW architecture to study the optical injection of spin-polarized electrons in $Al_{0.22}Ga_{0.78}As$ material over the excitation energy range of 1.85–3.4 eV using a Xenon arc lamp (average power density $\sim 4\text{mW/cm}^2$). Based on the results, it was established that, although the magnitude of the DCP is determined by QW parameters, its spectral dependence is solely governed by the barrier layer and is identical to the bulk material. In this paper, we extend the method to indirect bandgap materials since the radiative recombination of carriers can occur efficiently in the QW layer. Spin relaxation of photo-injected electrons in the *X* valley of indirect bandgap AlGaAs epilayers is successfully measured in the 10–80 K range. Theoretical framework along with associated experiments are discussed with an aim of the measurement of τ_S^X influenced by k-linear Dresselhaus spin splitting, which is found to be an order of magnitude higher than τ_S^L.

The rest of this paper is organized as follows. In Sec. II, a theoretical model based on the capture of electrons in QWs via different valleys, Γ to QWs in direct and Γ-*X* to QWs in indirect AlGaAs barrier layers, is proposed. The corresponding rate equations are solved to estimate the steady-state spin-polarized carrier density in barrier and QW layers. Timescales of different phenomena like intervalley scattering, spin relaxation, quantum capture, and carrier recombination are included in the rate equations to explain the experimental observations. Section III contains the sample details and experimental methods that are used for characterization. Section IV consists of miscellaneous experimental results, theoretical calculations based on DFT, and comparison of the estimated value of τ_S^X. Analysis of excitation energy and temperature-dependent electron spin dynamics is also included in this section. Further, Sec. V brings forth a summary of the work presented in this paper.

II. THEORETICAL MODELING

The rate equation model developed by Stanton and Bailey [24] and then extended by Mudi *et al.* [32] estimates the steady-state distribution of photoexcited spin-polarized electrons in different valleys of the conduction band by considering different scattering and relaxation mechanisms viz. spin and energy relaxation, carrier capture in QWs, and carrier recombination. Here, we have further extended this model, to obtain a steady-state expression for the DCP of PL signal originating from the QW layer. Note that the model of Mudi *et al.* [32] excludes the dynamics of photogenerated holes due to their ultrafast spin relaxation time [9]. In this context, it is necessary to evaluate the photogenerated spin-polarized electron population (n_S^{QW}) as well as total electron population ($n_{\text{Total}}^{\text{QW}}$) in the ground state of the QW layer for the cases of photoexcitation in barrier and QW layers. One can derive an expression for the DCP from the ratio of these two quantities.

Since we are interested in the electron spin dynamics in the barrier material, the contribution arising from the QW must be ruled out. Therefore, the rate equations are solved for photoexcitation in the barrier as well as in the QW and the contribution from QWs is carefully separated out. Further, Pfalz *et al.* [33] have derived an expression to understand how initial spin relaxation during energy relaxation from the higher states of QWs affects the measured value of the DCP. According to their calculations, the fraction of electrons (R)

which can retain their initial spin polarization after reaching the QW ground state is given by the formula [33]

$$R = 1 - \left(\frac{2\pi\tau_E}{T_Z}\right)^2, \tag{1}$$

where τ_E is the energy relaxation time within the QW, which is of the order of 100 fs [33], and T_Z is the average spin relaxation time of electrons in the QW excited states [33]. For thick QWs, T_Z is estimated to be less sensitive to electron kinetic energy (E_K) than thin QWs [33]. For a 15-nm-thick QW, the calculated value of T_Z is ∼10 ps for $E_K = 75$ meV. These parameters yield the numerical value of R to be 0.996. From this, one can conclude that, for thick QWs, photogenerated electrons preserve significant spin polarization, while energy relaxation and the two-level rate equation will be sufficient to understand their dynamics, the two levels being the ground state of the barrier and the QW. In this context, the ascribed rate equation can be written as

$$\frac{d}{dt}\begin{pmatrix} n_S^B \\ n_S^{\mathrm{QW}} \end{pmatrix} = \begin{bmatrix} -(\gamma_C + \gamma_S^B) & 0 \\ \gamma_C & -\gamma_S^{\mathrm{QW}} \end{bmatrix}\begin{pmatrix} n_S^B \\ n_S^{\mathrm{QW}} \end{pmatrix} + \begin{pmatrix} GP_0 \\ 0 \end{pmatrix}, \tag{2}$$

where n_S^B is the steady-state photogenerated spin-polarized electron population in the barrier layer, γ_C and $\gamma_S^B(\gamma_S^{\mathrm{QW}})$ stand for the electron capture rate from the barrier to the QW ground state and the electron spin relaxation rate in the barrier layer (QW ground state), respectively. Further, G and P_0 are the photogeneration rate and the instantaneous degree of spin polarization (DSP) of photogenerated electrons in the barrier layer, respectively. Note that γ_S^{QW} also incorporates the loss of electron spin due to the electron-hole recombination in QWs. More precise expression for γ_S^{QW} would be $\gamma_S^{\mathrm{QW}} = \gamma_S^{\mathrm{pure}} + \gamma_R^{\mathrm{QW}}$. Here, γ_S^{pure} and γ_R^{QW} are the pure spin relaxation rate and electron recombination rate in the QW ground state. Now from the steady-state solution of Eq. (2), one can easily acquire

$$\begin{pmatrix} n_S^B \\ n_S^{\mathrm{QW}} \end{pmatrix} = G\begin{bmatrix} \frac{P_0}{(\gamma_C+\gamma_S^B)} \\ \frac{P_0\gamma_C}{\gamma_S^{\mathrm{QW}}(\gamma_C+\gamma_S^B)} \end{bmatrix}. \tag{3}$$

Further, to derive an expression for $n_{\mathrm{Total}}^{\mathrm{QW}}$, all spin relaxation channels should be put to zero, and P_0 should be equal to 1. This gives rise to the expression

$$\begin{pmatrix} n_{\mathrm{Total}}^B \\ n_{\mathrm{Total}}^{\mathrm{QW}} \end{pmatrix} = \begin{pmatrix} \frac{G}{\gamma_C} \\ \frac{G}{\gamma_R^{\mathrm{QW}}} \end{pmatrix}. \tag{4}$$

Thus, the formula to evaluate the DCP of the PL signal coming from the QW for photoexcitation in the barrier is written as

$$\mathrm{DCP} = \frac{n_S^{\mathrm{QW}}}{n_{\mathrm{Total}}^{\mathrm{QW}}} = \frac{P_0}{\left(1+\frac{\gamma_S^{\mathrm{pure}}}{\gamma_R^{\mathrm{QW}}}\right)\left(1+\frac{\gamma_S^B}{\gamma_C}\right)}. \tag{5}$$

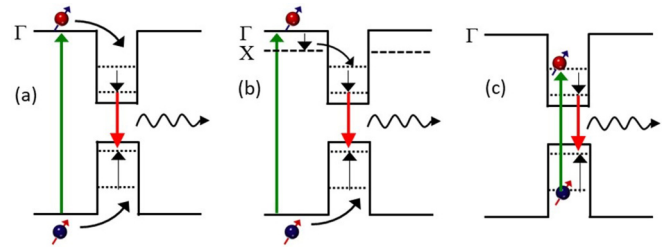

FIG. 1. Schematic diagram of electron capture and recombination in an AlGaAs/GaAs quantum well (QW) for photoexcitation in the (a) direct band gap barrier, (b) indirect band gap barrier, and (c) QW.

This expression is quite like the DCP expression obtained by other researchers for a two-level system [22], indicating the accuracy of the rate equation model presented here.

A. Direct band gap AlGaAs barrier

A pictorial representation of the electron spin dynamics for the direct band gap AlGaAs barrier is shown in Fig. 1(a). In this case, electrons are photogenerated in the Γ valley of the AlGaAs barrier which are directly captured by the QW after diffusion and subsequent quantum capture via interaction with optical phonons. Thus, the expression of the DCP for photoexcitation in the barrier layer can be written as

$$\mathrm{DCP}^{\Gamma} = \frac{n_S^{\mathrm{QW}}}{n_{\mathrm{Total}}^{\mathrm{QW}}} = \frac{P_0}{\left(1+\frac{\gamma_S^{\mathrm{pure}}}{\gamma_R^{\mathrm{QW}}}\right)\left(1+\frac{\gamma_S^{\Gamma}}{\gamma_C}\right)}. \tag{6}$$

Here, γ_S^B is replaced with γ_S^{Γ} as the electron spin dynamics is limited in the Γ valley of the AlGaAs barrier. The superscript Γ with the DCP term is defined to highlight that the carriers are being captured from the Γ valley of the AlGaAs barrier.

B. Indirect band gap AlGaAs barrier

For the indirect band gap AlGaAs barrier, the electron spin dynamics is slightly different. Here, electrons are photoexcited in the Γ valley, which lies above the satellite L and X valleys in the E-k diagram. Since in indirect band gap AlGaAs, the conduction band minimum (CBM) lies near the X point, photoexcited electrons will eventually thermalize to the X valley via an energy relaxation process, which makes it a multilevel system. Therefore, writing a closed-form equation like Eq. (5) is not straightforward. In this case, it is necessary to determine the steady-state spin-polarized carrier population in the Γ, L, and X valleys before being captured by the QW. Note that the thermalization procedure here might occur via a single-step (Γ to X) or dual-step (Γ to L and then L to X) process. The ascribed rate equations are

$$\frac{d}{dt}\begin{pmatrix} n_S^{\Gamma} \\ n_S^{L} \\ n_S^{X} \end{pmatrix} = \begin{bmatrix} -(\gamma^{\Gamma-L}+\gamma^{\Gamma-X}+\gamma_S^{\Gamma}) & 0 & 0 \\ \gamma^{\Gamma-L} & -(\gamma^{L-X}+\gamma_S^{L}) & 0 \\ \gamma^{\Gamma-X} & \gamma^{L-X} & -\gamma_S^{X} \end{bmatrix}\begin{pmatrix} n_S^{\Gamma} \\ n_S^{L} \\ n_S^{X} \end{pmatrix} + \begin{pmatrix} GP_0 \\ 0 \\ 0 \end{pmatrix}, \tag{7}$$

where n_S^I and γ_S^I are the density of the spin-polarized carriers and spin relaxation rate in the Ith valley, respectively, and γ^{I-J} stands for the intervalley scattering rate from the Ith to the Jth valley. Other symbols have their usual meaning. By solving these rate equations, the steady-state carrier density in different valleys (n_S^Γ, n_S^L, n_S^X) can be estimated. Further, the fractional population of the spin-polarized carriers can be realized by the expression

$$\begin{pmatrix} f_S^\Gamma \\ f_S^L \\ f_S^X \end{pmatrix} = \begin{bmatrix} \frac{n_S^\Gamma}{(n_S^\Gamma+n_S^L+n_S^X)} \\ \frac{n_S^L}{(n_S^\Gamma+n_S^L+n_S^X)} \\ \frac{n_S^X}{(n_S^\Gamma+n_S^L+n_S^X)} \end{bmatrix} = \begin{bmatrix} \frac{\gamma_S^X(\gamma^{L-X}+\gamma_S^L)}{(\gamma^{L-X}\gamma_S^X+\gamma_S^X\gamma_S^L+\gamma^{\Gamma-L}\gamma_S^X+\gamma^{L-X}\gamma^{\Gamma-L}+\gamma^{\Gamma-X}\gamma^{L-X}+\gamma^{\Gamma-X}\gamma_S^L)} \\ \frac{\gamma^{\Gamma-L}\gamma_S^X}{(\gamma^{L-X}\gamma_S^X+\gamma_S^X\gamma_S^L+\gamma^{\Gamma-L}\gamma_S^X+\gamma^{L-X}\gamma^{\Gamma-L}+\gamma^{\Gamma-X}\gamma^{L-X}+\gamma^{\Gamma-X}\gamma_S^L)} \\ \frac{\gamma^{L-X}\gamma^{\Gamma-L}+\gamma^{\Gamma-X}\gamma^{L-X}+\gamma^{\Gamma-X}\gamma_S^L}{(\gamma^{L-X}\gamma_S^X+\gamma_S^X\gamma_S^L+\gamma^{\Gamma-L}\gamma_S^X+\gamma^{L-X}\gamma^{\Gamma-L}+\gamma^{\Gamma-X}\gamma^{L-X}+\gamma^{\Gamma-X}\gamma_S^L)} \end{bmatrix}. \tag{8}$$

Here, f_S^I indicates the fractional population of spin-polarized carriers in the Ith valley. Finally, by putting $\gamma_S^X = 4 \times 10^{11}$ s^{-1} (theoretically calculated value explained in the next section), $\gamma_S^L = 5 \times 10^{12}$ s^{-1} (Ref. [22]), $\gamma^{\Gamma-X} = 2 \times 10^{13}$ s^{-1} (Ref. [34]), $\gamma^{\Gamma-L} = 8.3 \times 10^{12}$ s^{-1} (Ref. [34]), and $\gamma^{L-X} = 4 \times 10^{12}$ s^{-1} (Ref. [35]), the numerical values of f_S^Γ, f_S^L, and f_S^X turn out to be 0.015, 0.015, and 0.97 respectively. These results are a consequence of faster Γ-X intervalley scattering time whose value is ~50 fs for the current scenario (Ref. [34]). As a result, both Γ and L valleys of the indirect band gap AlGaAs barrier will play a minimal role in the attribution of the electron spin dynamics, and most of the electrons will not lose their spin information before reaching the X valley. A similar concept is found in the case of indirect band gap germanium, where electrons are scattered from the Γ valley to the L valley [36]. Therefore, it is safe to assume that photogeneration of spin-polarized carriers is taking place only in the satellite X valley, and the Γ and L valleys have a very minimal role to play. Thus, the electron spin dynamics can again be evaluated by a two-state model, as depicted in Fig. 1(b). In this context, the expression for the DCP of PL is given by

$$\mathrm{DCP}^X = \frac{n_S^{\mathrm{QW}}}{n_{\mathrm{Total}}^{\mathrm{QW}}} = \frac{P_0}{\left(1+\frac{\gamma_S^{\mathrm{pure}}}{\gamma_R^{\mathrm{QW}}}\right)\left(1+\frac{\gamma_S^X}{\gamma_C^X}\right)}, \tag{9}$$

where symbols have their usual meaning, and the superscripts with the symbols identify the region of occupation of photogenerated electrons. This expression is very similar to the expression of the DCP derived for direct band gap barriers [Eq. (6)], except that γ_S^Γ is replaced by γ_S^X, representing the different capture path of the photogenerated electrons in the barrier, while the contribution coming from the QW remains the same. Further, it should be emphasized that, in the present model, X-Γ intervalley scattering is completely ignored. This assumption is valid only for $Al_xGa_{1-x}As$ alloys with higher aluminum composition ($x > 0.5$). This is because, near the Γ-X crossover ($x = 0.41$–0.5), a significant amount of X-to-Γ backscattering takes place due to the nature of the E-k band structure. As a result, the spin dynamics will be much more complicated, and the current expression for the DCP will not be valid.

Following a similar approach, one can derive an expression for the DCP of the PL when the photoexcitation is tuned to higher energy levels of QWs. The corresponding expression is specified as

$$\mathrm{DCP}^{\mathrm{QW}} = \frac{n_S^{\mathrm{QW}}}{n_{\mathrm{Total}}^{\mathrm{QW}}} = \frac{P_0'}{\left(1+\frac{\gamma_S^{\mathrm{pure}}}{\gamma_R^{\mathrm{QW}}}\right)}. \tag{10}$$

Notably, the electron spin dynamics for photoexcitation inside the QW remains invariant against the nature of the barrier bandgap, represented by Fig. 1(c). Therefore, the DCP of luminescence for photoexcitation inside the QW will be evaluated from Eq. (10) for both cases. Further, for this photoexcitation range, the value of instantaneous DSP (P_0') of photogenerated electrons will be different due to modified selection rules in the QW [33]. The contribution coming from the QW can be eliminated by taking the ratio of Eqs. (5) and (10):

$$\frac{\mathrm{DCP}}{\mathrm{DCP}^{\mathrm{QW}}} = \left(\frac{P_0}{P_0'}\right)\frac{1}{\left(1+\frac{\gamma_S^B}{\gamma_C}\right)}. \tag{11}$$

The QW contributions can differ for direct and indirect barrier samples because of (i) difference in the spin relaxation rate in QW layers, (ii) difference in compensation of unpolarized background electrons, and (iii) difference in electron recombination rate in the QW. As will be shown later, all these factors contribute only a little, which is further reduced after taking a ratio as defined by Eq. (11). Once the QW contributions are carefully separated out, one can estimate the electron spin relaxation time in the barrier ($\tau_S^B = 1/\gamma_S^B$) by putting in the numerical values of DCP, $\mathrm{DCP}^{\mathrm{QW}}$, P_0, P_0', and γ_C parameters. Among these, generally DCP, $\mathrm{DCP}^{\mathrm{QW}}$, and γ_C are measured experimentally, whereas P_0 and P_0' are known from the selection rules.

III. METHODS

Due to compensation of unpolarized background electrons without inducing additional ionized impurity scattering, p-type modulation doping is an attractive technique to enhance the magnitude of the DCP of the luminescence signal arising from QWs [23]. Hence, the samples under investigation were p-type modulation-doped $GaAs/Al_xGa_{1-x}As$ single QWs with QW width (d_{QW}) of 15 nm. The aluminum (Al) composition of the barrier layer was kept at 0.26, 0.37, and 0.63 for the three samples labeled as S1, S2, and S3, respectively. Further, a $GaAs/Al_xGa_{1-x}As$ multi-QW sample marked as S4 was also included in the investigation. This sample contained four QWs of thicknesses 2.3, 4, 8.3, and 15 nm and had Al composition of 0.63 in the barrier layer. All samples were grown on $n^+ - GaAs$ substrate (001) by MOVPE, where trimethyl gallium, trimethyl aluminum, and arsine were used as precursors to grow epitaxial layers. To achieve p-type doping, trimethyl zinc was used as the dopant. Further, a 10 nm GaAs cap layer was grown on top of each sample to prevent the oxidization of the AlGaAs barrier layer.

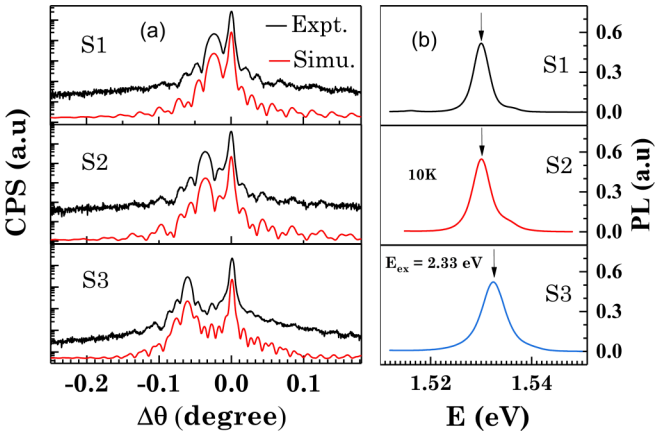

FIG. 2. (a) High-resolution x-ray diffraction (HRXRD) pattern of GaAs/$Al_xGa_{1-x}As$ single quantum well (QW) samples. (b) 10 K photoluminescence (PL) spectra of QW samples at $E_{ex} = 2.33$ eV, where the vertical arrow on the PL peak indicates the detection energy for photoluminescence excitation (PLE) experiments.

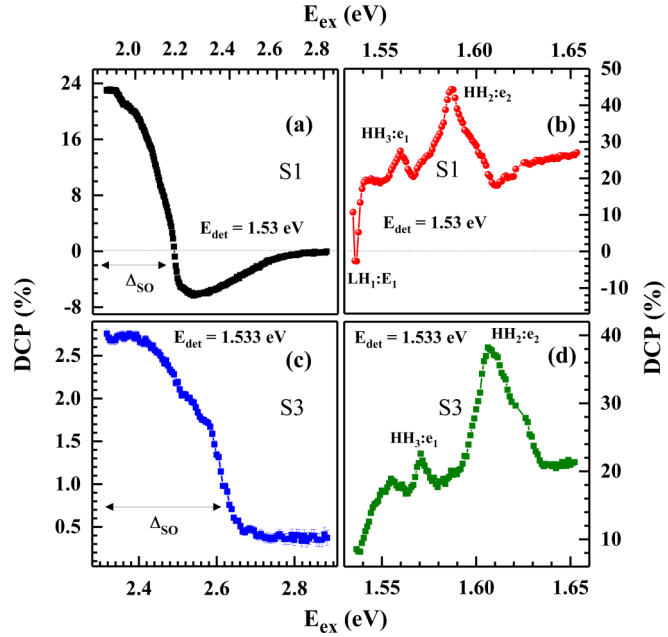

FIG. 3. 10 K degree of circular polarization (DCP) spectra of S1 sample for (a) excitation in the barrier and (b) excitation in the quantum well (QW), and of S3 sample for (c) excitation in the barrier and (d) excitation in the QW. Here, E_{det} indicates the detection energy at which the DCP spectra is measured.

In the sample design, a spacer layer of 25 nm thickness was incorporated to separate the Zn dopants from the QW. The layer was reasonably thin for the accumulation of holes in the QW but large enough for the suppression of ionized impurity scattering [37]. The numerical value of dopant density inside the QW for S3 was determined by the capacitance-voltage method and was estimated to be 1.65×10^{12} cm^{-2} at 300 K. The dopant density in other samples was kept in a similar range. QW width and Al composition of these samples were evaluated by high-resolution x-ray diffraction (HRXRD) and PLE spectroscopy techniques. Pendellösung fringes observed in the HRXRD pattern, as shown in Fig. 2(a), indicate about a high crystalline quality of the samples. The samples are also characterized using a PL technique as illustrated in Fig. 2(b), where primarily the electron-heavy-hole excitonic peak is observed at 10 K. The lower intensity electron-light-hole excitonic peak indicates that the hole accumulation is minimal but is sufficient to compensate the available free background electrons. From the width of excitonic peaks, interface fluctuation of a few monolayers was estimated in all samples [38]. Note that the usage of QW architecture of high crystalline quality significantly enhances the signal strength, thereby enabling measurement of a few percent DCP even at very low excitation intensity, which is generally obtained from broad band sources like a xenon arc lamp. In our case, an average power density of only 4 mW/cm^2 at 630 nm was used in the measurements. The samples were mounted on the cold head of a helium-based closed-cycle refrigerator which could operate in the 10–300 K temperature range. The details of the experimental setup are published elsewhere [23]. Here, the DCP-measured PL signal was estimated by the formula $\mathrm{DCP} = F\frac{(I^+ - I^-)}{(I^+ + I^-)}$, where I^+ (I^-) are the PL intensity related to co (counter)-polarized excitation. Here, F is the calibration factor which takes care of the misalignment of optics and frequency response of the measurement system, and its value is estimated to be 3.3 for our current experimental setup.

IV. RESULTS AND ANALYSIS

The DCP of the PL signal was measured for S1 and S3 samples at different values of excitation energy to investigate the electron relaxation properties. Representative 10 K DCP spectra are shown in Figs. 3(a) and 3(c) for photoexcitation in the barrier and in Figs. 3(b) and 3(d) for the excitation in the QW layer. It can be seen from Figs. 3(b) and 3(d) that, in the case of photoexcitation inside the QW, the shape of the DCP spectra for two samples remains the same apart from a shift in the energy scale due to change in the confinement potential. Peaks associated with various QW transitions are marked in the figure, which match with those observed in photoreflectance spectra (not shown here) and are also found to agree with the eigenvalues obtained by solving the Schrödinger equation. A similar magnitude of the DCP for both samples indicates the robustness of the electron spin dynamics for photoexcitation inside the QW, irrespective of the difference in the nature (value) of band structure (band gap) of the barrier layer. On the other hand, by comparing the DCP spectra of S1 and S3 for barrier excitation, one can note two important differences: (i) for near band-edge excitation, the magnitude of the DCP in S3 is reduced by an order as compared with that of S1, (ii) the sign of the DCP spectra is opposite in S1 and S3 beyond excitation energy $E_{ex} = E_g + \Delta_{SO}$. Here, ($E_g$) and Δ_{SO} stand for the band gap and split-off gap near the zone center ($k = 0$), respectively. Accordingly, the impacts of the electron spin dynamics on the DCP spectra in these two regimes are explained separately. The results from the first regime are used to estimate τ_S^X and its temperature dependence. Theoretical calculations were also performed to corroborate with the experiments. On the

other hand, the results from the second regime demonstrate the impact of the X valley on the hot electron spin dynamics.

A. Estimation of τ_S^X

For near band-edge photoexcitation, the DCP spectra is determined by electrons with low kinetic energy; therefore, energy relaxation in the barrier material need not be considered. Hence, the discussion mainly involves the electron capture path from the barrier to the QW and simultaneous spin relaxation at various energy states inside the QW. However, as explained earlier, the latter component is quite similar in both samples. In this context, a mismatch in the DCP magnitude for S1 and S3, as shown in Figs. 3(a) and 3(c), can be ascribed to one of the following reasons: (i) a difference in the spin relaxation rate in the barrier layers or (ii) a difference in the carrier capture rate from the barrier to the QW. The two factors are represented by γ_S^B and γ_C parameters, respectively, in Eq. (11). In the literature, capture of electrons through both Γ and X valleys is studied in detail for AlGaAs/GaAs QWs, and the reported value of capture time $\tau_C(\tau_C = 1/\gamma_C)$ is ~20 ps [39–41]. Thus, from the measurement of DCP and DCP^{QW}, and by using Eq. (11), the value of electron spin relaxation time $(\tau_S^B = 1/\gamma_S^B)$ in the AlGaAs barrier can be estimated. Following the proposed method, the value of τ_S^B is measured for S1, which contains the AlGaAs barrier of the direct band gap (Γ valley) nature. Note that the procedure requires the values of P_0 and P_0' also. Since P_0 deals with bulk barrier material, its value is taken to be 50%, which is decided by angular momentum selection rules. On the other hand, Pfalz *et al.* [33] have theoretically calculated the magnitudes of P_0' for photoexcited electrons associated with different transitions in GaAs QWs. According to their calculations, $P_0' = 82.5\%$ for the [heavy hole (HH)] HH_2-e_2 transition in QWs with $d_{\text{QW}} = 15$ nm. For S1, this transition is observed at $E_{\text{ex}} = 1.587$ eV in Fig. 3(b), and the value of $\text{DCP}^{\text{QW}} = 44.4\%$. Similarly, following near barrier-band-edge photoexcitation in Fig. 3(a), the value of DCP is ~23%. Thus, by putting these values in Eq. (11) and taking $\tau_C = 20$ ps, one can obtain $\tau_S^B = 1/\gamma_S^B = 118 \pm 1$ ps. It is in good agreement with the values of τ_S^B estimated by other researchers for AlGaAs through time-resolved PL and with the values reported for GaAs whose band structure is like that of direct band gap AlGaAs [22,42]. To further crosscheck the validity of the proposed method for the measurement of τ_S^B, we have selected the HH_3-e_1 transition in the QW ($P_0' = 51.6\%$, $\text{DCP}^{\text{QW}} = 27.5\%$) and obtained $\tau_S^B = 126 \pm 1$ ps. Thus, any higher transition showing a well-defined peak in DCP spectra can be utilized for this purpose. However, Pfalz *et al.* [33] have stated that thick QWs are preferred for this purpose since, in that case, the spin relaxation during the thermalization of electrons via the excited states of QW is minimal.

We have followed a similar method to determine the electron spin relaxation time in the barrier layer of S3. Note that the electron spin dynamics will be governed by the satellite X valley due to the indirect nature of the barrier band gap. The DCP spectra for photoexcitation in the barrier and QW layers are illustrated in Figs. 3(c) and 3(d), respectively. In this case, though the magnitude of P_0 remains 50%, the value of DCP^X turns out to be only 2.76%. Following the same procedure and considering the $\text{HH}_2 - e_2$ transition, where $P_0' = 82.5\%$, $\text{DCP}^{\text{QW}} = 38.2\%$ and $\tau_C^X = 1/\gamma_C^X = 20$ ps, the estimated value of $\tau_S^X = \frac{1}{\gamma_S^X}$ turns out to be 2.7 ± 0.1 ps. If we consider the $\text{HH}_3 - e_1$ transition with $P_0' = 51.6\%$ and $\text{DCP}^{\text{QW}} = 22.7\%$ in place of the $\text{HH}_2 - e_2$ transition, then the value of τ_S^X turns out to be 2.9 ± 0.1 ps. This further validates the proposed method. Here, the value of τ_S^X has been measured in bulk III–V semiconductors where the electrons are delocalized. Notably, the magnitude of τ_S^X for delocalized electrons is six orders lower in magnitude than that of localized electrons [25,26]. This can be understood by considering efficient electron spin relaxation mechanisms such as D-P and E-Y mechanisms. Unlike localized electrons, the wave vector k is a good quantum number for delocalized electrons resulting in an efficient spin relaxation (approximately picosecond range) through these mechanisms. Similar observation has also been made in GaAs quantum dots where electron spin relaxation time reaches milliseconds [4], a six- to seven-order rise in magnitude compared with their bulk counterpart, where typical spin relaxation time lies in the hundreds of picoseconds range at low temperature [22].

It is surprising to note that even theoretical predictions for τ_S^X in the bulk are not available in the literature. Here, the same is tried out by considering D-P spin relaxation under k-linear Dresselhaus spin splitting regime [43] and is discussed in the next subsection of this paper.

B. Theoretical framework for the estimation of τ_S^X

In Ref. [43], it was already described that the D-P spin relaxation time under k-linear Dresselhaus spin splitting can be calculated by using the following relation:

$$\tau_S = \frac{\hbar^4}{8 m_t \beta_D{}^2 k_B T \tau_p}, \tag{12}$$

where ħ, m_t, β_D, k_B, T, and τ_P stand for the reduced Planck's constant, transverse effective mass of electrons, Dresselhaus spin-orbit coefficient, Boltzmann's constant, temperature, and momentum relaxation time, respectively. Since the X valley of AlGaAs also comprises k-linear Dresselhaus spin splitting [44], this formula could be used to estimate the numerical value of τ_S^X at 10 K. A typical value of $\tau_P = 370$ fs for the near band-edge excitation is theoretically estimated at 10 K for the X valley of AlGaAs considering polar optical phonon scattering, alloy scattering, equivalent inter-X-valley scattering, deformation potential scattering, piezoelectric scattering, and ionized impurity scattering in the calculations. One can calculate the X-valley electron mobility (μ^X) using the expression $\mu^X = \frac{e\tau_P}{m_e^X}$ to crosscheck the value of τ_P. With $m_e^X = 0.278 m_0$, the low-temperature value of μ^X turns out to be $0.023\ \text{m}^2\text{V}^{-1}\text{s}^{-1}$, which is very close to the one reported for a similar composition of AlGaAs [45]. Further, to estimate the numerical value of β_D^X, DFT-based electronic structure calculations were carried out using the plane-wave basis [46]. We took an energy cutoff (E_{cut}) of 500 eV. The exchange correlation functional was approximated by the Perdew-Burke-Ernzerhof version of the generalized gradient approximation [47]. For the sampling of the Brillouin zone, we used a Monkhorst-Pack mesh of $5 \times 5 \times 5$ k-points. The

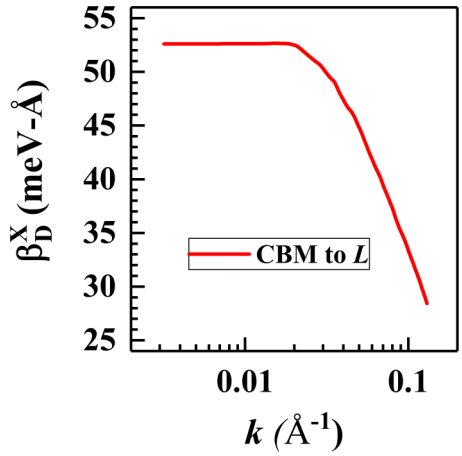

FIG. 4. X-valley Dresselhaus spin-orbit coefficient along the conduction band minimum (CBM) to L is plotted as a function of wave vector k.

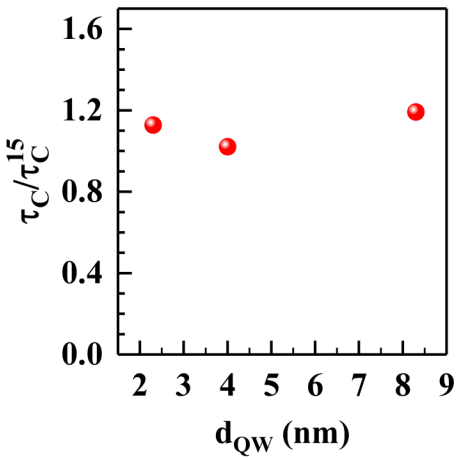

FIG. 5. Variation of estimated electron capture time in S4 plotted as a function of quantum well (QW) width.

convergence criterion for energy in the self-consistent-field cycle was taken to be 10^{-6} eV. To simulate the material close to the experimental stoichiometry, we used a supercell where the required number of Al atoms were replaced by Ga atoms. Various possible configurations were considered to find out the lowest energy structure, and the band structure was calculated for that energetically lowest configuration. The band structure was calculated using a set of discrete k points around the CBM. The band splitting energy for the nth band with a momentum k was estimated by taking the energy difference between the bands split due to the spin-orbit coupling. The X-valley Dresselhaus spin-orbit coefficient was calculated by using the formula [18] $\beta_D^X = \frac{\Delta E(k)}{2k}$, where ΔE is the spin-orbit splitting near the CBM, and k is the lattice wave vector. The variation of β_D^X against the wave vector k is illustrated in Fig. 4. Note that the $k = 0$ point in the plot is set as the CBM where β_D^X is found to be constant at 52 meV/ Å before a gradual fall at higher k values. This variation is like the one observed in GaAs [18]. The CBM value of β_D^X was used in the calculations since, in steady state, the electrons thermalize to the CBM. Other parameters like $m_t^x = 0.205m_0$ (m_0 is the free electron mass), $T = 10$ K, $k_B = 1.38 \times 10^{-23}$ J/K were used to get the 10 K numerical value of τ_S^X to be 2.3 ps, which is found to be in good agreement with the values measured in the previous section. It is worth mentioning that Eq. (12) is derived for bulk material without strain, where only Dresselhaus splitting is considered. However, presence of strain brings an additional spin-orbit term, which is also k linear in nature [48]. In the present sample, the $Al_{0.63}Ga_{0.37}As$ layer was pseudomorphically grown on a GaAs substrate, and a residual strain of only 0.08% was measured. It might alter the estimated value of τ_S^X, but the difference is expected to be rather small, and the same was therefore neglected in theoretical calculations. Further, DFT calculations were carried out by assuming an ideal system at 0 K temperature, which can lead to some difference between the theory and experiments. Furthermore, a better match can be obtained by considering a slightly lower value of τ_C, which is possible for the samples grown under different conditions.

C. Temperature dependence of τ_S^X

The temperature dependence of τ_S^X can be studied by analyzing the behavior of the DCP spectra as a function of temperature. Before doing that, the temperature sensitivity of τ_C should be clearly addressed. The temperature variation of τ_C depends upon the nature of electron capture, which can be either classical, i.e., a process governed by the drift and diffusion of electrons, or quantum mechanical, i.e., a process governed by resonant quantum capture. One possible way to figure out the dominant mechanism is to look for the dependence of τ_C on width (d_{QW}) of the QW. Notably, for classical electron capture, the value of τ_C does not depend upon the d_{QW}, unlike the quantum capture process where a clear oscillation against d_{QW} is generally observed [40]. To identify the governing mechanism, we grew a multi-QW sample, where QWs with four values of thickness, i.e., $d_{QW} = 2.3, 4, 8.3$, and 15 nm were grown in a sample labeled as S4. Measurements and analysis were repeated for S4 like single-QW samples. Since the barrier material was the same for all QWs, τ_S^B can be taken to be the same for all of them. Further, using Eq. (11), the ratio $\frac{\tau_C}{\tau_C^{15}}$ was estimated and is plotted in Fig. 5. Note that the parameter τ_C^{15} stands for the electron capture time in a 15-nm-thick QW. A near unity value of $\frac{\tau_C}{\tau_C^{15}}$, irrespective of different values of d_{QW}, indicates a move toward the classical capture process of electrons in this sample. It was already shown that, for thick barriers like in our sample, electrons are captured through a classical process which is robust against temperature over the 10–300 K range [49,50]. Thus, no temperature variation is anticipated for τ_C. Since the barrier structure of S3 is identical to S4, the electron capture dynamics in S3 is also expected to be similar.

Therefore, by keeping $\tau_C = 17$ ps for comparison purposes, the temperature dependence of τ_S^X was studied over the 10–80 K range, and the same is plotted in Fig. 6, where a monotonous fall of τ_S^X is observed. Shortening of the electron spin relaxation time with temperature has been reported earlier, and the same is explained by considering the enhancement of the thermal velocity of electrons [13]. A large enhancement in the thermal velocity of electrons is responsible

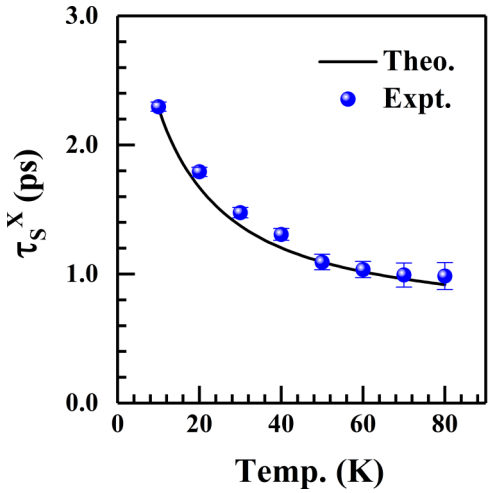

FIG. 6. Temperature dependence of τ_S^X in S3 sample. Black solid line addresses the same for theoretically calculated values.

for the rise of the effective magnetic field arising from Dresselhaus spin-orbit coupling. Due to this factor, a fall in the values of the electron spin relaxation time is noticed with temperature. This factor is represented by the temperature term in the denominator of Eq. (12). However, the power law for the temperature dependence of τ_S^X, i.e., of $\tau_S^X \propto T^\alpha$, is primarily governed by the variation of τ_P with temperature. For the present case, the estimated value of α is ~ -0.4, indicating that τ_P varies as $T^{-0.6}$. Interestingly, no scattering mechanism supports such a temperature dependence of τ_P. Only alloy scattering, piezoelectric scattering, and inter-X-valley scattering mechanisms come close to such a trend where $\tau_P \propto T^{-0.5}$ [51]. Among these scattering mechanisms, the inter-X-valley scattering is calculated to be the fastest one and exhibits a numerical value of 700 fs at 10 K. Similar conclusions are already available in the literature for GaAs [52]. Hence, it is expected that the main contribution of τ_P usually comes from equivalent inter-X-valley scattering. A minor difference observed between the experimental and theoretical values of α can be explained by considering the effect of residual strain in AlGaAs layers due to the lattice mismatch with the GaAs substrate. van Kesteren *et al.* [53] have shown that heteroepitaxial strain-induced band structure modification in AlAs layers, keeping the growth direction along the z axis, lifts the degeneracy in the X valley in such a way that (X_z) lies above (X_x) and (X_y) on the energy scale. For $Al_{0.63}Ga_{0.37}As$, the energy separation between (X_z) and X_x/X_y is $\sim$10 meV. Thus, at very low temperature (10–40 K), the equivalent inter-X-valley scattering will take place between (X_x) and (X_y) only. However, with the rise of temperature, the role of (X_z) in the inter-X-valley scattering will also become important. In this context, the inter-X-valley scattering time formula can be written as [51]

$$\frac{1}{\tau_{XX}} = \frac{Z_f D_{XX}^2 (m_e^*)^{3/2} (k_B T)^{1/2}}{\pi\sqrt{2}\rho\omega_{\rm LO}\hbar^3}[N + (N+1)], \qquad (13)$$

where Z_f, D_{XX}, m_e^*, N, ρ, and $\omega_{\rm LO}$ stand for the number of final valleys available for scattering, X-valley deformation potential field, effective mass of electrons in the X valley, phonon number, mass density of AlGaAs, and longitudinal optical phonon angular frequency, respectively. In the present scenario, Z_f itself depends on temperature, and its variation can be understood by the expression

$$Z_f = \left[1 + \exp\left(-\frac{\Delta E_X}{k_B T}\right)\right], \qquad (14)$$

where ΔE_X is the energy separation between (X_z) and X_x/X_y. At high temperature, the value of Z_f increases significantly, and it makes the temperature variation of τ_P faster than anticipated. This is the reason why the temperature dependence of τ_S^X in Fig. 6 deviates from $\alpha = 0.5$, especially when the temperature is > 50 K.

D. Impact on hot electron spin dynamics

From numerous studies of hot electron spin dynamics in the Γ valley, the D-P spin relaxation enhances with the kinetic energy of electrons [31]. One can conveniently inject hot electrons in the conduction band by keeping the energy of the impinging photons much larger than the band gap of semiconductors. Consequently, the DCP spectra generally fall with excitation energy, and the nature of spectra is expected to depend on the spin splitting and energy relaxation time. Since for the X valley these two parameters are significantly different from the Γ valley, the corresponding DCP spectra are expected to be different, particularly at high excitation energy. One of the key differences between the two cases is seen for $E_{\rm ex} = E_g + \Delta_{\rm SO}$, where the observed 10 K DCP spectra of S1 and S3 are of opposite sign, as shown in Figs. 3(a) and 3(c). Since the QW material and thickness are the same in the two samples, the difference is bound to be from the barrier material alone. Ekimov and Safarov [8] have pointed out that, in GaAs, the sign of the DCP spectra above $E_{\rm ex} = E_g + \Delta_{\rm SO}$ depends upon the dopant density of the sample, and it changes beyond a critical value of dopant density. However, in the present scenario, AlGaAs barriers are unintentionally doped ($<10^{15}$ cm^{-3}), except for the thin doped spacer layers. Thus, the different nature (direct vs indirect) of the band gap of AlGaAs barriers in S1 and S3 ought to be the fundamental reason behind this observation since the electrons are captured via the X valley in the latter case. To further crosscheck this observation, similar measurements were performed in S2 which bore an AlGaAs barrier of Al composition of 0.37. For this Al composition, the AlGaAs barrier is a direct band gap but very close to the Γ-X crossover [54]. Measured DCP spectra for this sample is shown in Fig. 7, and a clear negative value is observed beyond $E_{\rm ex} = E_g + \Delta_{\rm SO}$.

Note that the optical orientation properties of electrons near the Γ valley are well known and will clarify the physics behind these results. Here, the fall of the DCP with excitation energy can be explained by considering the transitions from various valence bands having different angular momentum. For near band-edge ($k = 0$) excitation energy, electrons are excited from heavy hole (HH) and light hole (LH) bands. At the Brillouin zone center ($k = 0$), both bands are equal weightage admixture of $|\frac{1}{2}, \frac{1}{2}\rangle$ and $|\frac{1}{2}, \frac{-1}{2}\rangle$ angular momentum states [10]. Calculations considering the selection rules lead to the fact that, for near the band edge, both HH and LH bands will generate electrons with 50% spin polarization. However,

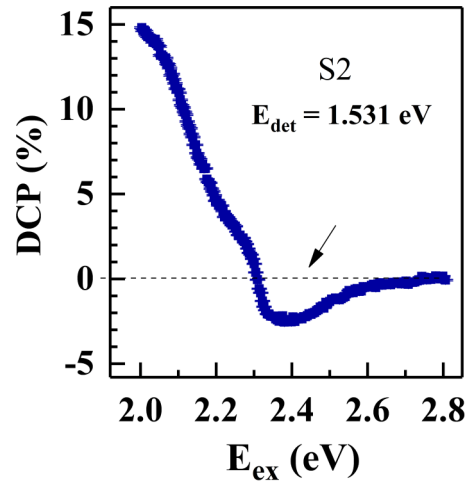

FIG. 7. 10 K degree of circular polarization (DCP) spectra of S2 sample.

with increase in photon energy (i.e., for transition involving larger k), the LH band acquires more and more split-off (SO) band character and therefore generates electrons with opposite spin polarization [10]. This will cause a decrease in the DSP of photogenerated electrons, and the same is reflected in the DCP spectra shown in Figs. 3 and 7.

To explain the experimental results beyond $E_{\rm ex} = E_g + \Delta_{\rm SO}$, we recall Eq. (5), which estimates the value of the DCP of luminescence for near band-edge excitation but excludes the electron spin loss during the thermalization process. However, for hot electrons, as in the present case, this process becomes much more important, and these equations will lead to erroneous values of the DCP. Thus, to invoke the physics of electron spin relaxation during their energy relaxation, Eq. (5) is to be modified as given below [23]:

$$\mathrm{DCP} = \frac{P_0 \exp\left[-\int_{E_{\rm th}}^{E_0} \frac{\gamma_S^B(E_k)}{\gamma_E^B(E_k)} \frac{dE_k}{E_k}\right]}{\left(1+\frac{\gamma_S^{\rm QW}}{\gamma_R^{\rm QW}}\right)\left(1+\frac{\gamma_S^B}{\gamma_C}\right)}, \tag{15}$$

where γ_E^B and E_k are the energy relaxation rate of electrons in the AlGaAs barrier and kinetic energy of photogenerated electrons, respectively. Here, E_0 and E_{th} stand for the kinetic energies of electrons at the time of photoexcitation and after reaching equilibrium, respectively. This expression is valid for both direct and indirect band gap AlGaAs barriers. The only difference is the region of operation of electrons which is the Γ valley for direct band gap AlGaAs and the X valley for indirect band gap AlGaAs. Further, this expression clarifies that the nature and the magnitude of DCP^{Γ} and DCP^{X} beyond $E_{\rm ex} = E_g + \Delta_{\rm SO}$ is a signature of kinetic-energy (E_K) dependence of the electron spin relaxation time, which is cubic for the Γ valley and linear for the X valley [23,44]. To appreciate this fact, 14-band $\mathbf{k}\cdot\mathbf{p}$ calculations were performed to estimate the band structure of AlGaAs. This computation reveals that, for photoexcitation near $E_g + \Delta_{\rm SO}$, the approximate kinetic energies of electrons generated from HH, LH, and SO bands are 150, 95, and 15 meV, respectively. In the case of the direct band gap AlGaAs barrier (S1, S2), electrons are captured in the QW through the Γ valley. As a result, two different bunches of photogenerated electrons are observed: (i) electrons generated from HH and LH bands with very high kinetic energy and (ii) electrons generated from the SO band near the band edge. In the former case, most of the electrons will lose their spin orientation even before reaching the QW. On the contrary, electrons in the latter case will remember their spin polarization, and thus, the DCP of luminescence will reflect a negative DSP character of the SO band. This result is a consequence of k^3 dependence of Dresselhaus spin splitting in the Γ valley, and more details about it are published elsewhere [23].

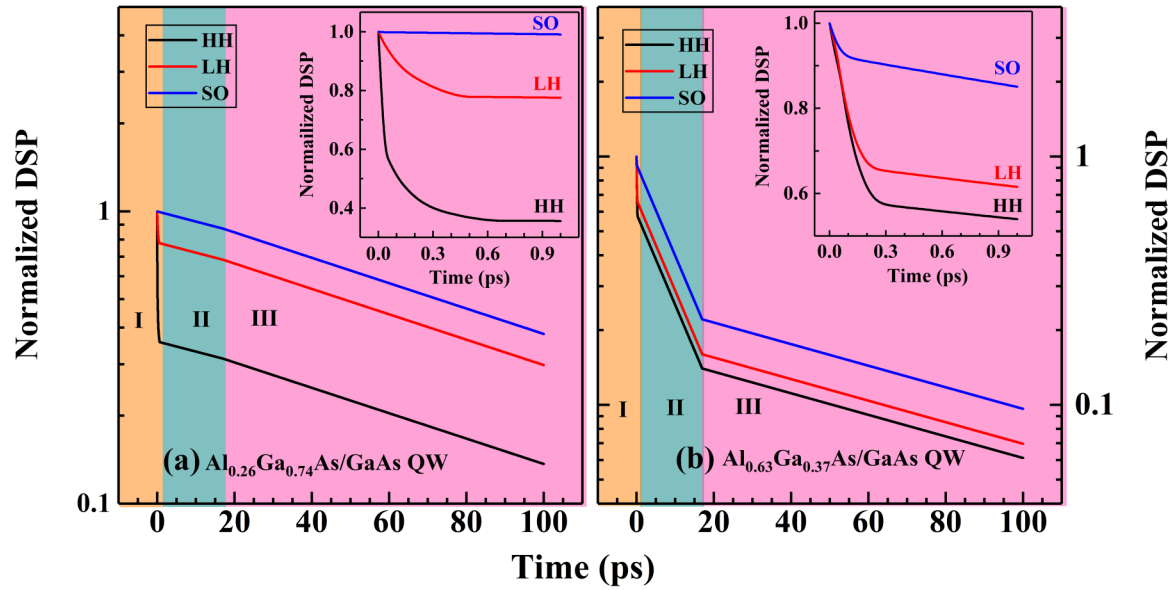

FIG. 8. Numerically calculated temporal evaluation of the degree of spin polarization (DSP) of the electron in (a) S1 and (b) S3; the respective insets show the magnified portion of initial data to clarify the effect of simultaneous energy and spin relaxation. The regions shaded as orange (I), indigo (II), and pink (III) represent different regimes of electron spin relaxation process.

This can be better appreciated if the DSP is plotted as the time evolution of the spin polarization of electrons excited from different bands. This is depicted in Figs. 8(a) and 8(b), which are divided into three parts, in accordance with the dynamics of the corresponding time regime. The regimes labeled as I (orange), II (indigo), and III (pink) are related to electron spin relaxation during thermalization, after being thermalized to the barrier band edge and in the QW, respectively. The initial part of the data is magnified and plotted as insets in the respective figure. The time axis is taken up to 100 ps, which is generally the carrier recombination time in the QW. Therefore, the normalized DSP at 100 ps is the DCP, which is observed experimentally. In S1 [Fig. 8(a)], the electrons generated from SO and LH valence bands can retain their spin polarization significantly, whereas those excited from HH bands lose it very quickly. Therefore, the observed DCP has negative polarity due to a dominant component of the DSP appearing from the SO band.

On the other hand, in S3, which consists of an indirect band gap AlGaAs barrier, the initial electron spin dynamics takes place in the satellite X valley, where the energy relaxation process is faster than that of the Γ valley [55]. Thus, electrons can be readily thermalized to the X-valley minimum irrespective of their kinetic energy, and the duration during which electrons simultaneously lose their spin polarization and energy becomes shorter, as shown in Fig. 8(b) and its inset. Further, due to linear k-dependent Dresselhaus spin splitting in the X valley, τ_S^X is less sensitive to E_K. Even though the numerical value of the DSP of electrons generated from the HH at 100 ps is slightly lower as opposed to that from LH and SO electrons, the larger value of photo-absorption in the former case maintains the positive polarity in the DCP spectra beyond $E_{\rm ex} = E_g + \Delta_{\rm SO}$. Therefore, the opposite polarity of DCP spectra at these excitation energies is directly correlated to the different nature of spin dynamics in Γ and X valleys.

V. SUMMARY AND CONCLUSIONS

In conclusion, the spin relaxation time of delocalized electrons in the X valley of indirect bandgap AlGaAs barrier layers was measured by analyzing the DCP of the PL signal of the QW layer, where the contribution from spin relaxation in the QW is carefully eliminated. Assuming a two-level model, an analytical expression relating the DCP of the PL signal and τ_S^X of the barrier layer was derived. Using this equation, τ_S^X was estimated to be 2.7 ± 0.1 ps, which is found to be in good agreement with the theoretical calculations based on DFT. The temperature dependence of τ_S^X was recorded in the 10–80 K range, which is explained by invoking D-P spin relaxation under the k-linear spin-splitting regime. It was found that intravalley scattering in strain-modified X valleys lying along the in-plane and transverse directions dominates the spin relaxation process. Further, the spin dynamics of photogenerated hot electrons is for both direct and indirect bandgap AlGaAs epitaxial layers. The distinct nature of the DCP curve beyond $E_{\rm ex} = E_g + \Delta_{\rm SO}$ for the two cases is explained by considering faster energy relaxation and linear Dresselhaus spin splitting in the satellite X valley. The indirect band nature of $Al_{0.63}Ga_{0.37}As$, where accumulation of spin-polarized carriers is feasible in the X valley, even in the absence of external bias, provides an excellent opportunity for the development of spin devices with adequate Joule heating. The enhanced value of τ_S^X, which is an order of magnitude higher than τ_S^L, is expected to help in the optical manipulation of spin devices. Furthermore, the procedure elaborated here will be applicable in the case of other group III–V and group IV indirect bandgap semiconductors and is expected to be useful in understanding the role of phonon-assisted processes in the spin polarization of electrons.

ACKNOWLEDGMENTS

The authors acknowledge Dr. V. K. Dixit and Ms. Geetanjali for their help in sample growth and useful discussions. Technical support received from Mr. U. K Ghosh, Mr. Sanjay Porwal, and Mr. Alexandar Khakha is also acknowledged. The authors further acknowledge the contribution of Dr. D. Pandey in the DFT calculations and thank the Computer Division, RRCAT, for support in installing and smooth running of the code. P.M. and J.B. thank Homi Bhabha National Institute for financial support.

[1] A. E. Giba, X. Gao, M. Stoffel, X. Devaux, B. Xu, X. Marie, P. Renucci, H. Jaffrès, J.-M. George, G. Cong, Z. Wang, H. Rinnert, and Y. Lu, Phys. Rev. Appl. **14**, 034017 (2020).

[2] N. Nishizawa, K. Nishibayashi, and H. Munekata, Proc. Natl. Acad. Sci. **114**, 1783 (2017).

[3] M. Lindemann, G. Xu, T. Pusch, R. Michalzik, M. R. Hofmann, I. Žutic, and N. C. Gerhardt, Nature (London) **568**, 212 (2019).

[4] M. Kroutvar, Y. Ducommun, D. Heiss, M. Bichler, D. Schuh, G. Abstreiter, and J. J. Finley, Nature (London) **432**, 81 (2004).

[5] N. Nishizawa, K. Nishibayashi, and H. Munekata, Appl. Phys. Lett. **104**, 111102 (2014).

[6] M. I. Dyakonov and V. I. Perel, Sov. Phys. JETP **33**, 1053 (1971).

[7] V. L. Vekua, R. I. Dzhioev, B. P. Zakharchenya, and V. G. Fleisher, Sov. Phys. Semicond. **10**, 210 (1976).

[8] A. I. Ekimov and V. I. Safarov, JETP Lett. **13**, 495 (1971).

[9] F. Meier and B. P. Zakharchenya, *Optical Orientation* (North Holland Press, Amsterdam, 1984).

[10] F. Nastos, J. Rioux, M. Strimas-Mackey, B. S. Mendoza, and J. E. Sipe, Phys. Rev. B **76**, 205113 (2007).

[11] M. Dyakonov, *Spin Physics in Semiconductors* (Springer, New York, 2008).

[12] M. D'Alessandro and D. Sangalli, Phys. Rev. B **102**, 104437 (2020).

[13] G. Fishman and G. Lampe, Phys. Rev. B **16**, 820 (1977).

[14] J. H. Buß, T. Schupp, D. J. As, D. Hägele, and J. Rudolph, J. Appl. Phys. **126**, 153901 (2019).

[15] M. Idrish Miah, J. Phys. D: Appl. Phys. **40**, 1659 (2007).

[16] R. Mallory, M. Yasar, G. Itskos, A. Petrou, G. Kioseoglou, A. T. Hanbicki, C. H. Li, O. M. J. van't Erve, B. T. Jonker, M. Shen, and S. Saikin, Phys. Rev. B **73**, 115308 (2006).

[17] S. Saikin, M. Shen, and M.-C. Cheng, J. Phys.: Condens. Matter. **18**, 1535 (2006).

[18] J. Y. Fua, M. Q. Weng, and M. W. Wu, Physica E **40**, 2890 (2008).

[19] N. Okamoto, H. Kurebayashi, T. Trypiniotis, I. Farrer, D. A. Ritchie, E. Saitoh, J. Sinova, J. Masek, T. Jungwirth, and C. H. W. Barnes, Nat. Materials **13**, 932 (2014).

[20] P. Mudi, S. K. Khamari, and T. K. Sharma, Phys. Status Solidi RRL **14**, 2000097 (2020).

[21] P. Mudi, S. K. Khamari, and T. K. Sharma, J. Phys. D: Appl. Phys. **54**, 205101 (2021).

[22] T. T. Zhang, P. Barate, C. T. Nguyen, A. Balocchi, T. Amand, P. Renucci, H. Carrere, B. Urbaszek, and X. Marie, Phys. Rev. B **87**, 041201(R), (2013).

[23] S. K. Khamari, P. Mudi, S. Porwal, and T. K. Sharma, J. Lumin. **213**, 204 (2019).

[24] C. J. Stanton and D. W. Bailey, Phys. Rev. B **45**, 8369 (1992).

[25] T. S. Shamirzaev, J. Rautert, D. R. Yakovlev, J. Debus, A. Yu. Gornov, M. M. Glazov, E. L. Ivchenko, and M. Bayer, Phys. Rev. B **96**, 035302 (2017).

[26] T. S. Shamirzaev, J. Rautert, D. R. Yakovlev, M. M. Glazov, and M. Bayer, Phys. Rev. B **99**, 155301 (2019).

[27] J. Debus, T. S. Shamirzaev, D. Dunker, V. F. Sapega, E. L. Ivchenko, D. R. Yakovlev, A. I. Toropov, and M. Bayer, Phys. Rev. B **90**, 125431 (2014).

[28] V. Yu. Ivanov, T. S. Shamirzaev, D. R. Yakovlev, A. K. Gutakovskii, Ł. Owczarczyk, and M. Bayer, Phys. Rev. B **97**, 245306 (2018).

[29] J. Rautert, T. S. Shamirzaev, S. V. Nekrasov, D. R. Yakovlev, P. Klenovský, Yu. G. Kusrayev, and M. Bayer, Phys. Rev. B **99**, 195411 (2019).

[30] M. S. Kuznetsova, J. Rautert, K. V. Kavokin, D. S. Smirnov, D. R. Yakovlev, A. K. Bakarov, A. K. Gutakovskii, T. S. Shamirzaev, and M. Bayer, Phys. Rev. B **101**, 075412 (2020).

[31] D. S. Smirnov, T. S. Shamirzaev, D. R. Yakovlev, and M. Bayer, Phys. Rev. Lett. **125**, 156801 (2020).

[32] P. Mudi, S. K. Khamari, and T. K. Sharma, J. Appl. Phys. **126**, 065703 (2019).

[33] S. Pfalz, R. Winkler, T. Nowitzki, D. Reuter, A. D. Wieck, D. Hägele, and M. Oestreich, Phys. Rev. B **71**, 165305 (2004).

[34] W. B. Wang, R. R. Alfano, D. Szmyd, and A. J. Nozik, Phys. Rev. B **46**, 15828 (1992).

[35] W. B. Wang, Kai. Shum, R. R. Alfano, D. Szmyd, and A. J. Nozik, Phys. Rev. Lett. **68**, 662 (1992).

[36] F. Pezzoli, F. Bottegoni, D. Trivedi, F. Ciccacci, A. Giorgioni, P. Li, S. Cecchi, E. Grilli, Y. Song, M. Guzzi, H. Dery, and G. Isella, Phys. Rev. Lett. **108**, 156603 (2012).

[37] P. J. van Hall, Superl. and Micrstr. **6**, 213 (1989).

[38] S. Haldar, V. K. Dixit, G. Vashisht, S. K. Khamari, S. Porwal, T. K. Sharma, and S. M. Oak, Sci. Rep. **7**, 4905 (2017).

[39] G. C. Crow and R. A. Abram, Semicond. Sci. Technol. **14**, 1 (1999).

[40] J. E. M. Haverkort, P. W. M. Blom, P. J. Van Hall, J. Claes, and J. H. Wolter, Phys. Status Solidi B **188**, 139 (1995).

[41] H. Schneider and E. C. Larkins, Solid State Electron. **40**, 133 (1996).

[42] E. V. Kozhemyakina, K. S. Zhuravlev, A. Amo, D. Ballarini, and L. Viña, Appl. Phys. Lett. **95**, 182107 (2009)

[43] T. Zhang, Spin injection in systems based on semiconductors III-V with a view to new spintronic components, Ph.D. Thesis, Université de Toulouse, 2014.

[44] S. Mishra, S. Thulasi, and S. Satpathy, Phys. Rev. B **72**, 195347 (2005).

[45] N. Chand, T. Henderson, J. Klem, W. T. Masselink, R. Fischer, Y.-C. Chang, and H. Morkoĉ, Phys. Rev. B **30**, 4481 (1984).

[46] G. Kresse and D. Joubert, Phys. Rev. B **59**, 1758 (1999).

[47] J. P. Perdew, K. Burke, and M. Ernzerhof, Phys. Rev. Lett. **77**, 3865 (1996).

[48] M. W. Wu, J. H. Jiang, and M. Q. Weng, Phys. Rep. **493**, 61 (2010).

[49] R. Kersting, R. Schwedler, K. Wolter, K. Leo, and H. Kurz, Phys. Rev. B **46**, 1639 (1992).

[50] B. Deveaud, J. Shah, T. C. Damen, and W. T. Tsang, Appl. Phys. Lett. **52**, 1886 (1988).

[51] A. K. Saxena and K. S. Gurumurthy, J. Phys. Chem. Solids. **43**, 801 (1982).

[52] M. K. R. Vyas, G. D. Pitt, and R. A. Hoult, J. Phys. C: Solid State Phys. **6**, 285 (1973).

[53] H. W. van Kesteren, E. C. Cosman, P. Dawson, K. J. Moore, and C. T. Foxon, Phys. Rev. B **39**, 13426 (1989).

[54] I. Vurgaftman, J. R. Meyer, and L. R. Ram-Mohan, J. Appl. Phys. **89**, 5815 (2001).

[55] N. Tandon, L. R. Ram-Mohan, and J. D. Albrecht, J. Elec. Materials. **47**, 7191 (2018).